High-Throughput Craze Studies in Gradient Thin Films Using Ductile Copper Grids

Alfred J. Crosby,† Michael J. Fasolka, and Kathryn L. Beers*

Polymers Division, National Institute of Standards and Technology, 100 Bureau Drive Stop 8542, Gaithersburg, Maryland 20899-8542

Received February 24, 2004; Revised Manuscript Received October 8, 2004

ABSTRACT: Polymer materials are being developed and used for numerous photonic and electronic applications where the polymer is expected to maintain its dielectric properties in confined geometries. In these applications, the initiation or growth of mechanically induced defects, such as crazes, cracks, or shear bands, can significantly alter the intended function of the polymer. In this paper, we introduce a high throughput methodology to facilitate the investigation of craze growth in confined films. Specifically, we extend the previous research conducted on the effects of film thickness on crazing of polystyrene into unexplored thickness regimes of films less than 100 nm. We combine novel techniques of gradient thin film preparation, the established methodology of the copper grid strain test, the automated features of atomic force microscopy, and batch image processing to provide increased throughput and standardization in our quantitative measurements. We demonstrate that the mechanisms of craze widening and micronecking are quantitatively continuous to film thicknesses as thin as 50 nm.

Introduction

Traditionally, studies of mechanically induced defects in polymers have concentrated on specimens for use in structural applications.[1−7] As polymers gain use as photonic and electronic materials, defects such as crazes, cracks and shear bands have increased importance. Although a degree of structural integrity is required in these applications, a more significant concern is the maintenance of the material's primary function, such as its dielectric properties. Crazes have different dielectric properties than the surrounding matrix, thus they will alter intended photonic and electronic properties. Moreover, in these applications, materials are not typically used as geometries where "bulklike" properties will necessarily dictate, they are often confined (e.g., as thin films, between particles in nanocomposites) to dimensions that approach the size of the polymer coil. Accordingly, as future technologies continue to push the dimensions of polymer applications to nanometer length scales, it is critical to explore thoroughly the consequences of severe confinement on polymer deformation processes, such as crazing.

While previous investigations provide a strong knowledge base for understanding the fundamental behavior of craze formation in thin films, much of the experimental work is limited to films of thickness greater than 100 nm. In this paper, we focus on crazing in polystyrene films in the thickess range 50−200 nm, which includes previously unexplored regimes of confinement. To accomplish this, we introduce a high-throughput methodology that not only facilitates this investigation of the effect of film thickness on crazing but also demonstrates a convenient and rapid approach for exploring the wide parameter space that has yet to be investigated.

Combinatorial and high-throughput methods have been used to advance several areas of materials science.[8] In this work, we employ *gradient techniques*, which rely on specimens that continuously vary in one or more parameters (e.g., thickness) as a function of position. Gradient combinatorial methods have been applied successfully to the study of several complex systems including polymer blends,[9] block copolymer films[10,11] and semicrystalline thin films.[12] In this work, we present an approach to observe and quantify craze structure in thin films of glassy polymers in a high throughput manner.

These measurements utilize the well-established copper grid technique,[1] modified to accommodate gradient specimens. Used extensively over the past 20 years, primarily by Kramer and colleagues,[1,2,4,7,13,14] the copper grid technique involves the uniaxial strain of a thin polymer film mounted onto a ductile copper grid. Observations of specimen deformation are achieved by monitoring the material suspended across the grid holes. The fracture processes within each grid space act independently and represent individual experiments.[1,4,5] Accordingly, as demonstrated in this paper, copper grid testing of gradient specimens enables parallel screening of craze behavior over a multitude of parameters. The use of gradient specimens increases efficiency while ensuring more reliable comparisons since the entire film library has an identical processing history.[9,15−19]

Although previous research on crazes concentrates on the use of transmission electron microscopy, we use atomic force microscopy (AFM) for craze analysis, since it yields direct quantitative measurement of craze structure,[20] and is adaptable to high-throughput approaches. Through automated analysis of AFM images, we are able to provide unique, thorough insight into polymer thin film crazing.

As noted above, our approach offers significant opportunities for the validation of new models by enabling systematic, comprehensive measurements over a large range of variable spaces.

Experimental Section[29]

Materials. Polystyrene ($M_r = 3 \times 10^5$, $M_r/M_n = 4.0$) and reagent grade toluene were purchased from Aldrich and used

* Corresponding author.
† Present address: Department of Polymer Science and Engineering, Conte Research Center, University of Massachusetts, 120 Governors Dr., Amherst, MA 01003.

10.1021/ma0496293
Published on Web 12/01/2004

Scheme 1

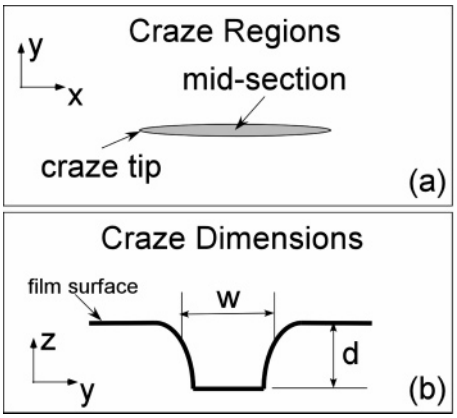

as received. A solution of 90% isotactic polystyrene (ipS) in toluene (mass fraction 4.5%) was obtained from Scientific Polymer Products ($M_r = 6 \times 10^5$, $M_r/M_n = 3.0$). Samples were diluted with toluene and filtered through 0.2 μm poly(tetrafluoroethylene) syringe filters before use. Copper grids (Copper 110, 20.32 μm thick, 50.8 lines per cm) were obtained from Buckbee-Mears (St. Paul, MN). Each grid space is approximately 1 mm^2.

Library Preparation. Films of gradient thickness were prepared using a flow coating method described previously[10,16] on 5 cm $\times$ 7.5 cm glass slides that had been cleaned in a UV/ozone chamber for 4 min. A solution of polymer in solvent was injected into the gap between a doctor blade and the substrate mounted on a computer-controlled translation stage. The stage/substrate was accelerated beneath the stationary blade, depositing steadily increasing volumes of solution along the substrate. Solvent evaporation results in a polymer film thickness gradient. The range and slope of the gradient are determined by the solution concentration (0.5−5% by mass fraction), gap height (50−250 μm), and the stage velocity profile (1−10 nm/min). The overall film dimensions were 3.5 cm $\times$ 5 cm. After the gradient film was deposited, the film was scored with a razor blade along the thickness gradient direction. Three incisions/scratches along the complete length of the film were made, and the center two strips were each 1.0 cm in width (Scheme 2). These center strips were marked with three fiduciary marks for alignment, and all strips were subsequently floated off onto water. The two edge strips were discarded to eliminate edge effects that are introduced during the flow coating process; the two center strips were transferred onto their respective substrates, one onto silicon and the other onto a treated copper grid.

The samples floated onto silicon were allowed to air-dry, and the thickness gradient was mapped using an UV−vis reflectance interferometer with a 0.5 mm spot-size mounted over two orthogonal robotic stages (Daedal) such that a two-dimensional array of points was obtained, spaced from 1 mm to 2 mm apart. These measurements were used to map the thickness (h) gradient across the copper grid samples using the fiduciary systems. The average variance in h across one grid space was estimated to be $\pm$3 nm. Representative data are shown as a surface plot in Figure 1.

Copper grids were cut into 2 cm $\times$ 8 cm strips, annealed in a furnace at 650 °C for 2 h, washed in hydrochloric acid, dipped in a 3% mass fraction solution of polystyrene in toluene, and dried prior to transferring the gradient samples. As discussed in previous papers,[1,7,13] precoating of the copper grid with PS enhances the adhesion between the copper grid and the floated PS film. In general, two gradient samples were transferred onto one copper grid for testing. The film supporting grids were exposed to toluene vapors for less than 1 min and dried in a vacuum oven overnight. This fabrication procedure is outlined in Scheme 2.

Measurements and Image Analysis. The copper grids with attached polymer films were strained on a Texture Analyzer (TA-XT2iHR) and held at 4% strain for a minimum of 10 min prior to removal. A video camera mounted on the Texture Analyzer recorded the onset of crazing. Upon removal, the plastic portion of the applied strain to the copper grid remains, and this strain is maintained in the attached polymer film. As in the conventional use of the copper grid technique, this feature allows us to qualitatively assess craze density, distribution and film integrity, in our case, using a Nikon Optiphot-2 microscope. We obtain multiple images of our combinatorial library by using two orthogonal robotic stages (Newport Corporation) and a Kodak Megaplus ES 1.0 CCD camera (1024 $\times$ 1024, 8-bit pixels) mounted to the optical microscope.

Craze microstructure was characterized by atomic force microscopy, which allows precise measurements of the craze dimensions, even very close to the tip. AFM micrographs were collected in tapping mode using a Digital Instruments Dimension 3100 (Nanoscope IIIa controller) and standard silicon cantilevers (Nanodevices) with a manufacturer-reported spring constant of approximately 30 N/m. To avoid specimen damage, AFM analysis of free-standing films requires low contact forces and slow scanning speeds. In this study, set point values were 85−90% of the cantilever free-air amplitude and scan rates were 0.25−0.5 μm/s. Image dimensions were 512 by 512 pixels.

AFM micrographs were acquired for up to three crazes in each grid square. Both craze tips and craze midsections (far from the tip) were examined (Scheme 1a). To standardize and provide statistical confidence in our quantitative measurements from the AFM micrographs, we built custom image-analysis routines with the IDL programming environment (Research Systems Inc.) to extract craze dimensions from the topography images in an automated manner. Craze depths and widths were measured via micrograph cross sections taken along the image lines oriented most perpendicular to the craze axis, so up to 512 measurements of a given dimension could be extracted from each micrograph. For each image line, a 10-pixel boxcar average was used to smooth the data. The craze depth (d) was then calculated as the difference between the maximum and minimum height values in the cross-section. Craze widths (w) were determined by identifying the positions of the craze edges in the cross-section (Scheme 1b). This was achieved by analyzing the local slope of the cross-section data, calculated along the image line using a simple difference function with a 5-pixel width. Craze edges represent the steepest features in the smoothed cross-section, so they are associated with the minimum and maximum values of the calculated derivative. For each image line, the positions of the craze edges were recorded. The craze widths were then calculated through a three-step process, which is necessary since generally the craze was not oriented exactly perpendicular to the image axes (as in Figure 1). First, a projected craze width (w_p) was calculated for each image line using the distance between the craze edge positions. Next, all of the positions of one craze edge (e.g., the points defining the left edge) were fit to a line via regression analysis. The angle (α) of this line with respect to the image axes was used to generate a correction factor ($\cos(\alpha)$) that accounts for the tilt of the craze. A final corrected craze width (w_r) was then calculated for each line where $w_r = \sin(\alpha)w_p$.

For micrographs of craze midsections, 512 measurements of w and d were averaged to yield the mean dimensions. These values were further averaged over the number of crazes measured in each grid (up to 3). For craze-tip micrographs, a user-identified craze-tip position enabled the analysis of craze dimensions as a function of distance from the tip. For measurements of d, this distance was calculated from the tip position, and the position of the minimum of the given image cross section. In the case of w, the distance was calculated using the tip position and the position of the craze midpoint, determined from the craze-edge location identified for each line. To better compare tips from films of different h, d, and w, data of craze tips for a given h were normalized using the average d and w determined from craze midsections with the same h. In cases where average values are reported (midsection analysis) and error bars are not included, the uncertainty in our measurements is less than 5%. Near the tip, w has a

Scheme 2

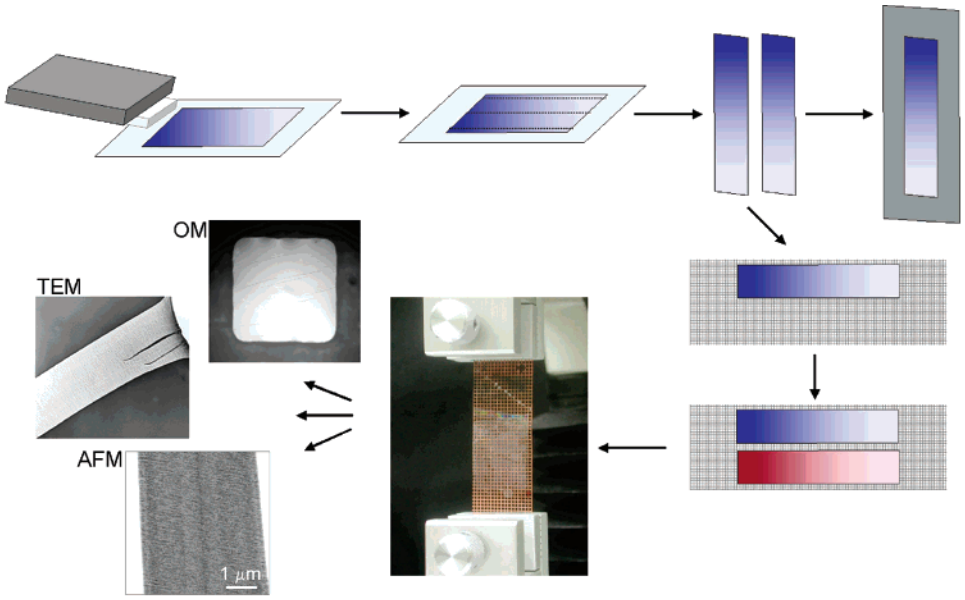

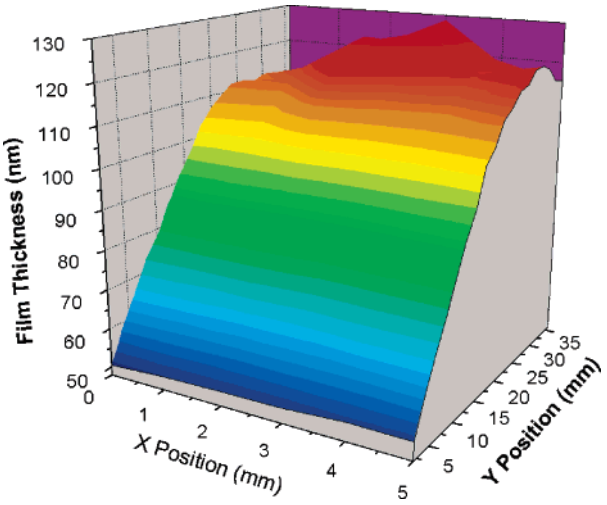

Figure 1. Surface plot of the thickness of a polystyrene gradient film cast by flow coating on glass and measured on silicon using spot interferometry.

standard uncertainty of 12% and d has a standard uncertainty of 15%. Two standard deviations from the values reported for the distance from the tip is 50 nm.

Background: Crazes in Thin Polymer Films

Crazes are discrete zones of stretched and voided material (i.e., fibrillar structures) that form perpendicular to an applied tensile stress.[5] The onset of crazing, although still not conclusively proven, is related to local hydrostatic stresses that cause void growth and can occur at strains as low as 0.7%.[1,5,14,21,22] Upon further straining, Saffman−Taylor instability[23] fingers develop in yielded material ahead of the craze tip and "pinch" (Figure 2) to form discrete bundles (i.e., fibrils) as the craze structure propagates.[5,14,24] For polystyrene, typical fibril sizes range from 5 to 30 nm in bulk materials.[5] As the craze propagates, the structure also widens. The widening process is dominated by a surface drawing mechanism by which new polymer chains are drawn into the craze fibrils.[5,14,25] Recent work shows that micronecking processes account for some deformation during the widening of crazes.

Craze width is governed by numerous factors including temperature, solvent exposure, strain rate, stress state, polymer chain length, and the presence of heterogeneities.[5,14] One-dimensional confinement, that is, film thickness, represents a governing factor that is related to the stress state.

When comparing bulk and thin film behavior, it is hypothesized that for films below a critical thickness, plastic constraint in the through-film direction is eliminated.[13] For polystyrene (PS), this critical thickness is approximately 150 nm.[13] That is, for identical stress states, PS films with thickness greater than 150 nm show a craze microstructure that is similar to that of the bulk. In contrast, for PS films below 150 nm, the craze microstructure, described as a perforated sheet with craze fibril diameters of up to 100 nm,[13,14,26] is markedly different compared to the bulk. The volume fraction (ϕ) of the craze material in thin films is significantly greater ($\phi = 0.33-0.5$) in comparison to thick films ($\phi = 0.15-0.25$, as measured by transmission electron microscopy).[13]

Although 150 nm is approximately the critical thickness for PS, theoretical analysis by Krupenkin and Fredrickson demonstrates that the transition from a 2D to 3D craze formation is a function of strain rate, yield stress, and effective viscosity.[26] Krupenkin and Fredrickson, along with Chan et al., report that the true stress in the craze fibrils is lower than the equivalent stress in thicker films because the stress normal to the polymer film is eliminated.[13,26] Accordingly, the draw ratio of craze fibrils in thin films is lower since the strain hardening behavior for polymers, like polystyrene, is unaffected by film thickness.

Chan et al. conclude that the mechanism for craze thickening or widening still proceeds by a surface drawing mechanism. Recently, investigations using atomic force microscopy show that, in addition to surface drawing, craze deformation is a micronecking process.[20,27,28] In other words, as the craze widens, or thickens, the craze structure necks in the direction normal to the film thickness. The extent of necking is referred to as the craze depth. The craze depth increases until the craze width reaches a critical value, w_c.[20] Previous investigations demonstrate that the plateau

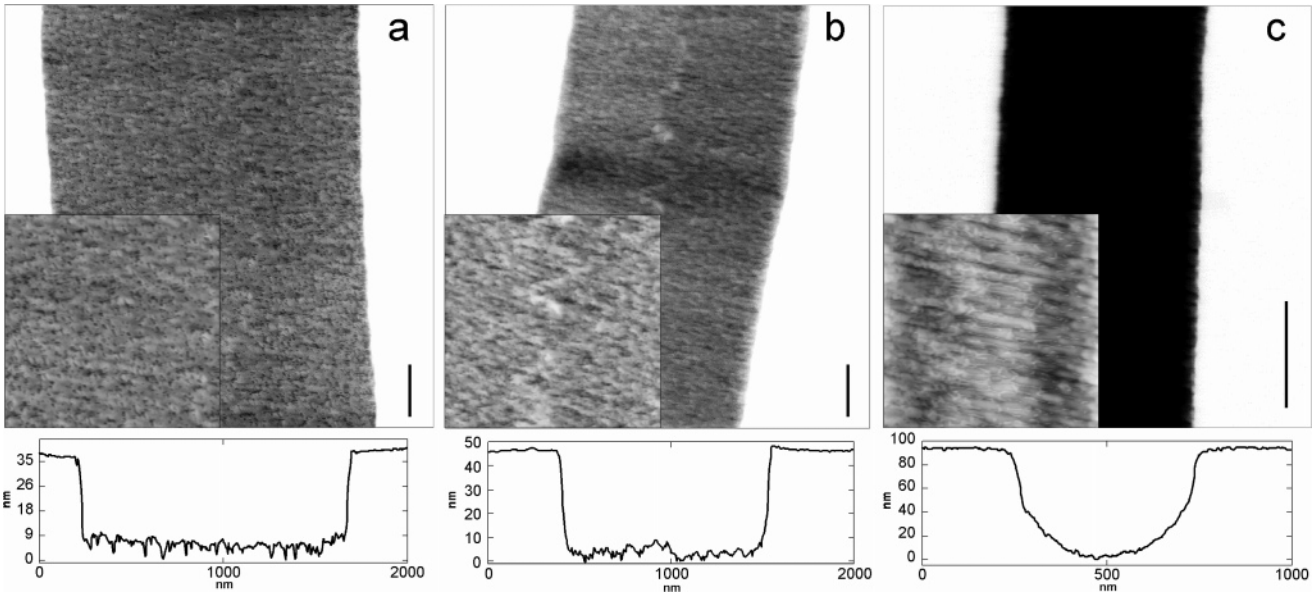

Figure 2. AFM topography images of representative craze midsections at three different film thicknesses; (a) $h = 78$ nm, (b) $h = 112$ nm, and (c) $h = 188$ nm. Insets show craze microstructure with higher contrast. Scale bar is 250 nm.

craze depth is linearly related to the film thickness for films greater than 120 nm, and w_c is dependent upon film thickness.[20] In addition to modifying the craze microstructure and micronecking processes, film thickness alters the mechanism of craze tip advancement.[13,26] In thick films, craze tips advance by a meniscus instability mechanism. In thin films, the craze tip follows a plastic deformation surface groove.

Results and Discussion

Combinatorial Methods. Combining gradient films with the well-known copper grid technique offers several advantages to study crazing in thin films. By varying the parameter of interest at small enough rates to provide comparatively uniform films across each grid square, the equivalent of up to 30 different films can be prepared, transferred, strained, and analyzed under identical conditions. This ability to analyze up to 30 combinations of craze-effecting variables on one sample eliminates many potential inconsistencies from film to film. These inconsistencies often arise from storing different samples in different environments (temperature and humidity) or preparing samples with slightly different processing conditions.

We used a single gradient in the films, which were wide enough (in the direction of uniform h) to cover approximately six grid spaces, so that statistics could be obtained across several spaces containing uniform films. Cutting away the edges of the cast film and using the center sections improved the symmetry of the films and reduced the variance across the nongradient direction. As Kramer and others have discussed previously, a primary advantage of the copper grid technique is the ability to collect statistical data on craze formation within a single film. To combine this advantage with combinatorial methodologies, we limit our libraries to one-dimensional gradients. In other words, we fabricate films with a thickness gradient in one direction. Although previous research has demonstrated the methods and advantages of using two-orthogonal gradients, we maintain uniform conditions orthogonal to the applied thickness gradient. This one-directional uniformity allows us to collect statistical data on craze growth. To further increase our throughput and single sample evaluation advantages, we combine two gradient films onto a single copper grid sample. This approach increases the number of simultaneous multivariable conditions that can be evaluated on a single sample.

Craze Midsection Analysis. The first of the two regions considered in our discussion is the midsection of the craze. Examples of images of craze midsections obtained on film segments with different h are shown in Figure 2. The crazes used for imaging were typically closer to the grid walls than the middle of the grid space. Weak oscillations in the suspended thin films lowered the stability of the tip/surface interactions, causing reduced sensitivity. To correct for this, the tendency was to use higher forces, which would rupture the brittle films. This problem was amplified in the center half of the grid square.

As h increases, so does the apparent depth of the craze (Figure 2c), making resolution difficult without manipulating the scale and contrast in the Nanoscope software. Significant use of the contrast is not recommended, however, since it can obscure the position of the side wall of the craze. In these images, only minor adjustment of the scale was used and subsections of the microstructure were extracted from the full craze image to resolve their structure (Figure 2, insets). In films with $h < 100$ nm, there is evidence of a perforated structure, rather than the fibril structure commonly reported in crazes in thicker films. The perforated structure has been observed previously[13] and theoretically described by Krupenkin and Fredrickson.[26]

IDL image analysis on batches of AFM files yielded precise measurements of dimensions of a given craze. Figure 3a contains data obtained from both measurements carried out using the Nanoscope software, choosing high and low points in the craze by eye, vs data generated by IDL. Good agreement is observed for both types of measurement, as well as across multiple samples with overlapping h gradients. Agreement was also observed between *amorphous* isotactic polystyrene and atactic polystyrene, providing good reference data to which semicrystalline samples[12] can be compared to measure the impact of crystalline ordering on structural

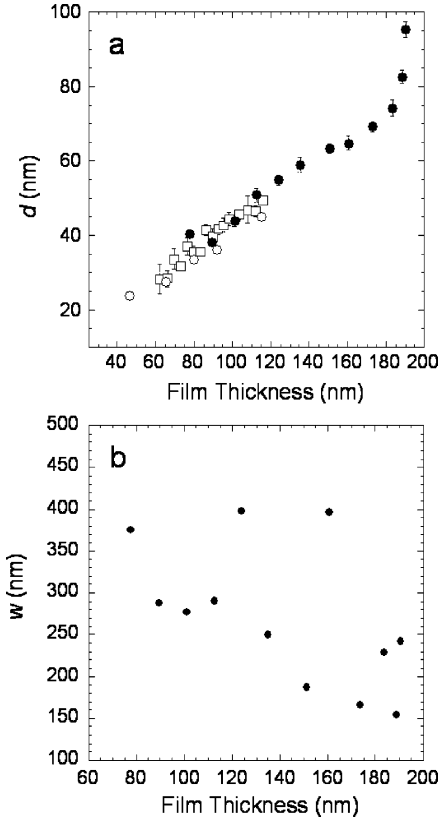

Figure 3. Craze midsection depth (a) and width (b) as a function of film thickness. Measurements were obtained on atactic polystyrene using cross-section analysis in Nanoscope (○) and IDL (●), as well as on isotactic polystyrene using IDL (□). Error bars represent two standards deviations in the average value of d.

integrity and material properties. The data indicate a nearly linear dependence of d on h within this thickness regime with the exception of the data points at $h > 180$ nm. It is the ability to obtain fast and consistent measurements on these samples across the thickness gradients that makes these data so convincing. One concern, however, is the trend at low h. If we were to assume that the crazes were symmetric normal to the plane of the film, then an extrapolation of our data would require the craze material to become increasingly thinner, approaching the single fibril dimensions observed in bulk materials (≈10 nm).

The linear dependence of craze depth with thickness for $h < 180$ nm is in good agreement with previous results. Yang et al. report that the ratio of craze depth to film thickness for a mature craze in a thin film saturates at a value of approximately 0.35.[20] The slope of our plot in Figure 3 gives a value of ≈0.37. In the research conducted by Yang et al.,[20] the ratio of 0.35 was limited to films at three film thicknesses: 120, 550, and 2600 nm. In contrast, our combinatorial gradient approach allows us to quantify this trend across a semicontinuous range of thickness values, thus increasing our statistical confidence in our conclusions.

The linear dependence displayed by our data is also significant in that it extends into film thicknesses of $h < 100$ nm. As discussed above, a change in the microstructure of the craze has been observed in film of thickness less than 100 nm. Although the stress state in this thickness regime no longer supports a hydrostatic stress component, the mechanism of micronecking in the crazed region still persists with the same

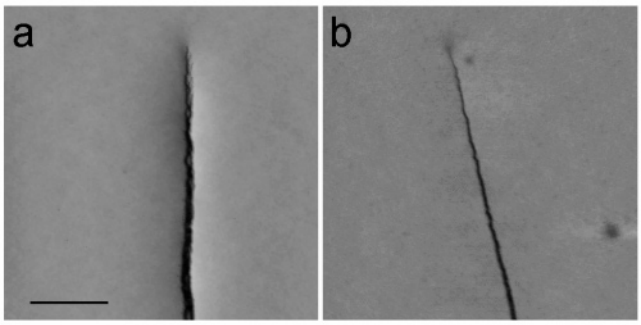

Figure 4. AFM topography image of a craze tip formed in a grid space with (a) $h = 78$ nm and (b) $h = 188$ nm. Scale bar is 500 nm.

dimensional stability. Our data quantitatively demonstrates this continuity in the micronecking process to thicknesses of at least 50 nm. While it would be useful to obtain more data at $h < 40$ nm, difficulty in transferring films in that regime onto the copper grids using the existing technique prevented us from obtaining the data. We were also interested in obtaining AFM images of the back of the film, however, the AFM head would not reach down inside the copper grid spaces.

For our measurements on films with $h > 180$ nm, the slope deviates from 0.33. In addition to craze depth, we examined the craze profile and craze width for the midsection region of the crazes. For all crazes in films with $h < 180$ nm, cross section analysis of the craze midsections showed mature crazes with smooth side walls and a flat fibril microstructure. This description of a mature craze has been previously reported.[20] Still weak variation in w was observed, both across the film and within individual grid spaces suggesting some dependence on local heterogeneity in the strain as expected; i.e., the degree of strain localization within the same grid square (Figure 3b). Although this variance was observed from craze to craze, our automated measurements of w for each craze midsection had negligible error associated with it.

For regions of our library where $h > 180$ nm at this global strain (3%), cross section analysis showed sloping walls dropping down to a rounded fibril region inside the craze in all of the AFM images obtained indicating early stage crazing as opposed to the well-developed structures found at lower h at this strain. This inconsistency in the strain-maturity of the crazes across our library may be attributed to processing conditions that introduce slight variations in the local strains within the different grid squares.

Craze Tip Analysis. A typical AFM height image of a craze tip in the thinner region of the film ($h = 78$ nm) is shown in Figure 4. The most apparent changes in microstructure for the craze tips in films with $h > 180$ nm were smoother edges and fewer islands of amorphous materials trapped inside the craze, although the depth profiles show significant difference (Figure 4b). When d was normalized for the maximum d of a given craze and plotted as a function of distance from the tip (Figure 5), we found that the crazes at smaller h approached the maximum d much faster.

These results are in agreement with Chan et al.[13] and Krupenkin and Fredrickson[26] who suggest that craze tip advancement follows a deformation zone or a surface groove that has been plastically deformed. In thinner films, the constraint in the direction normal to the film thickness is decreased. This diminishing constraint

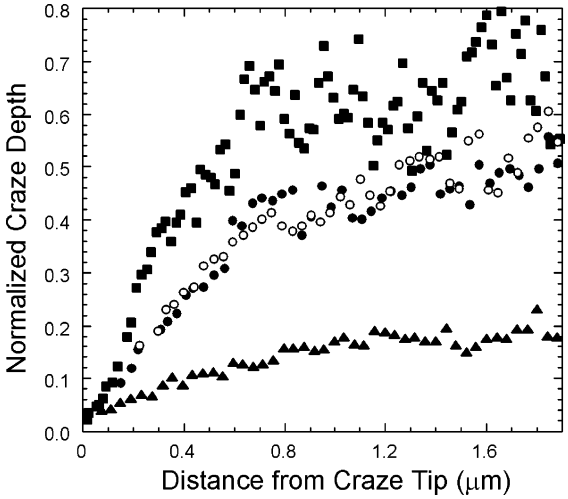

Figure 5. Craze depth as a function of distance from the craze tip. For comparison, depths have been normalized using midsection (maximum) depths for a given craze. h = 78 nm (■), h = 112 nm (○), h = 112 nm (●), and h = 188 nm (▲).

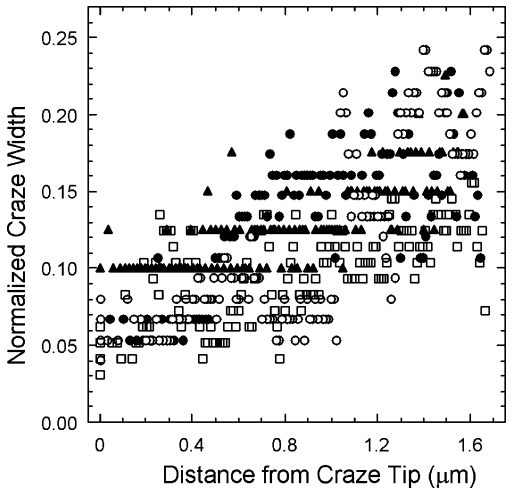

Figure 6. Craze width as a function of distance from the craze tip. For comparison, widths have been normalized using midsection (maximum) widths for a given craze. h = 78 nm (□), h = 112 nm (○), h = 112 nm (●), and h = 188 nm (▲).

increases the rate of micronecking in a plastically deformed region. In thicker films, the micronecking process is slower, and meniscus instabilities have time to form and collapse, thus forming craze fibrils. As the fibrils form, cross-tie fibrils provide for stress transfer through the thickness of the film and continue the micronecking process until the mature width of the craze, w_c, is achieved. As mentioned in previous investigations, and confirmed here for films below 120 nm, the nature of the polystyrene material properties is not changing.[13] Simply, the stress state is altering the balance of meniscus instability to micronecking mechanisms, thus the craze depth and microstructure are altered.

Although craze depth shows a strong dependence on distance from the craze tip, craze width shows a comparatively weak dependence (Figure 6). This indicates that the micronecking processes are dominating the early deformation processes over the craze thickening, or widening, process. This behavior is in agreement with the demonstration of Yang et al., which uses a sandwich film construction to suppress crazing in thin films. By restricting the early micronecking processes, the overall craze growth mechanism is delayed. Figure 6 also confirms that the widening process is not strongly influenced by h.

Conclusion

We have shown that combinatorial methods are effective tools for high throughput investigations of craze growth in thin polymer films. In the same samples, we have validated our test methods with previous results and tested a previously unexplored regime of thin film thickness. Our method includes preparation of gradient polymer thin films, the established copper grid strain test, and automated image analysis of AFM data. This method provides fast, quantitative characterization of craze dimensions in glassy polymer films. Our results show that for $h > 50$ nm, craze widening and micronecking mechanisms are quantitatively continuous.

Future work could sacrifice the statistical information provided in the orthogonal direction in a multivariable sample. For example, a polymer blend composition gradient orthogonal to a thickness gradient may provide unique and careful experimental data to support the work of Krupenkin and Fredrickson, who propose theoretical arguments regarding the effect of entanglement density on the critical thickness for polymer 3-D craze formation. Entanglement density is a parameter that can be controlled in a miscible polymer blend.

Acknowledgment. We thank Dr. A. P. Smith for providing TEM images on our samples.

References and Notes

(1) Lauterwasser, B. D.; Kramer, E. J. *Philos. Mag. A* **1979**, *39*, 469.
(2) Yang, A. C.-M.; Kramer, E. J.; Kuo, C. C.; Phoenix, S. L. *Macromolecules* **1986**, *19*, 2010.
(3) Brown, H. R. *Macromolecules* **1991**, *24*, 2752.
(4) Ryu, C. Y.; Ruokolainen, J.; Fredrickson, G. H.; Kramer, E. J. *Macromolecules* **2002**, *35*, 2157.
(5) Kramer, E.; Berger, L. *Fundamental Processes of Craze Growth and Fracture*; Kausch, H.-H., Ed.; Springer-Verlag: New York, 1990; Vol. 91/92, pp 1−68.
(6) Sauer, J.; Hara, M. *Fundamental Processes of Craze Growth and Fracture*; Kausch, H.-H., Ed.; Springer-Verlag: New York, 1990; Vol. 91/92, pp 69−118.
(7) Donald, A. M.; Kramer, E. J. *Philos. Mag. A* **1981**, *43*, 857.
(8) Meredith, J. C.; Karim, A.; Amis, E. J. *Mater. Res. Bull.* **2002**, *27*, 330.
(9) Meredith, J. C.; Karim, A.; Amis, E. J. *Macromolecules* **2000**, *33*, 5760.
(10) Smith, A. P.; Douglas, J. F.; Meredith, J. C.; Amis, E. J.; Karim, A. *J. Polym. Sci., Part B: Polym. Phys.* **2001**, *39*, 2141.
(11) Smith, A. P.; Douglas, J. F.; Meredith, J. C.; Amis, E. J.; Karim, A. *Phys. Rev. Lett.* **2001**, *87*, 015503−1.
(12) Beers, K. L.; Douglas, J. F.; Amis, E. J.; Karim, A. *Langmuir* **2003**, *19*, 3935.
(13) Chan, T.; Donald, A. M.; Kramer, E. J. *J. Mater. Sci.* **1981**, *16*, 676.
(14) Kramer, E. J. *Adv. Polym. Sci.* **1983**, *52−53*, 1.
(15) Smith, A. P.; Douglas, J. F.; Meredith, J. C.; Amis, E. J.; Karim, A. *J. Polym. Sci., Part B: Polym. Phys.* **2001**, *39*, 2141.
(16) Meredith, J. C.; Smith, A. P.; Karim, A.; Amis, E. J. *Macromolecules* **2000**, *33*, 9747.
(17) Jandeleit, B.; Schaefer, D. J.; Powers, T. S.; Turner, H. W.; Weinberg, W. H. *Angew. Chem., Int. Ed. Engl.* **1999**, *38*, 2494.
(18) Crosby, A. J.; Karim, A.; Amis, E. J. *J. Polym. Sci., Part B: Polym. Phys.* **2003**, *41*, 883.
(19) Cawse, J. N. *Acc. Chem. Res.* **2001**, *34*, 213.
(20) Yang, A. C. M.; Kunz, M. S.; Logan, J. A. *Macromolecules* **1993**, *26*, 1767.
(21) Argon, A.; Hannoosh, J. *Philos. Mag.* **1977**, *36*, 1195.
(22) Baljon, A. R. C.; Robbins, M. O. *Macromolecules* **2001**, *34*, 4200.

(23) Saffman, P. G.; Taylor, G. *Proc. R. Soc. London* **1958**, *245*, 312.
(24) Argon, A. S.; Salama, M. M. *Philos. Mag.* **1977**, *36*, 1217.
(25) Donald, A.; Kramer, E.; Bubeck, R. *J. Polym. Sci., Part B: Polym. Phys.* **1982**, *20*, 1129.
(26) Krupenkin, T. N.; Fredrickson, G. H. *Macromolecules* **1999**, *32*, 5029.
(27) Lin, C. H.; Yang, A. C. M. *J. Mater. Sci.* **2000**, *35*, 4231.
(28) Lin, C. H.; Yang, A. C. M. *Macromolecules* **2001**, *34*, 4865.
(29) Equipment and instruments or materials are identified in the paper in order to adequately specify the experimental details. Such identification does not imply recommendation by NIST, nor does it imply the materials are necessarily the best available for the purpose.

MA0496293